EDN: LPTQXH
УДК 535.211:536.331

Near-field Interaction Effects in Colloidal Au-CeYTbF$_3$ Nanoclusters in Plasmonic Immunoanalysis

Elina A. Izbasarova*
Almaz R. Gazizov†
Institute of Physics
Kazan Federal University
Kazan, Russian Federation

Received 13.11.2024, received in revised form 29.12.2024, accepted 04.02.2025

Abstract. In this paper, we study the effects of plasmonic enhancement of spontaneous emission in colloidal nanoclusters consisting of Au nanoparticles and CeYTbF$_3$ phosphor. Based on numerical simulation of various configurations of Au nanoparticles coated with polyethyleneimine, we analyzed the dependence of plasmonic resonances position on their number and distribution. The results showed that optimal nanoparticle configurations significantly enhance luminescence in the desired region of the visible spectrum, which opens up new possibilities for the development of highly sensitive nanosensors. At the same time, nanoclusters located on a Au substrate demonstrate a lower luminescence enhancement coefficient, while having a more inhomogeneous distribution of the optical near field. The results obtained reveal the dependence of the luminescence enhancement coefficient on the spatial distribution and coordination number of plasmonic nanoparticles in a nanocluster. This study contributes to the understanding of plasmonic interaction mechanisms and its applications in optical immunoassay and biomedical technologies.

Keywords: plasmonic nanoparticles, Purcell effect, Förster effect, FDTD modeling, luminescent nanoparticles.

Citation: E.A. Izbasarova, A.R. Gazizov, Near-field Interaction Effects in Colloidal Au-CeYTbF$_3$ Nanoclusters in Plasmonic Immunoanalysis, J. Sib. Fed. Univ. Math. Phys., 2025, 18(3), 347-357. EDN: LPTQXH.

Introduction

The scale of quantitative and dynamic analysis, which allows determining the state and behavioral characteristics of chemical and biological objects, is steadily growing [1]. Over the past decades, a number of electronic methods and devices have been developed for the detection of biomolecules. On the other hand, analysis based on the detection of photons rather than electrons is of growing interest to researchers due to the simplification of analytical instruments and their low cost. Moreover, optical analysis methods are more suitable for studying biological samples, are non-invasive and allow the sample to be examined under normal conditions. One such method is immunoassay based on the use of luminescent labels, the emission of which changes when an antigen with this label (refered to as probe when combined) is attached to the analyte [2]. Organic molecules are primarily used as labels in many areas of biomedicine. Nevertheless, despite the significant amount of research devoted to optical sensor systems using

*Izbasarova.E.A@mail.ru https://orcid.org/0000-0001-8300-4725
†equus.meteores@gmail.com https://orcid.org/0000-0002-9542-8856

organic probes, the difficulties associated with the preparation and production of such systems, as well as the photonic instability of organic materials, to some extent limit their practical application, especially in the context of long-term monitoring. In this regard, it seems advisable to develop stable optical systems based on new materials.

In the context dynamic progress in various fields of medicine, nanomaterials with a high specific surface area and unique optoelectronic properties are widely used for adsorption, in catalysis and analyte detection [3–5]. In particular, optical analysis based on plasmonic nanoparticles is applied to study various target objects, including chemical compounds, biomolecules, as well as physical characteristics such as temperature and viscosity to name a few [6–8]. Localized surface plasmon resonance (LSPR) in noble metal nanoparticles, associated with collective oscillations of free electrons, not only determines the color of the nanoparticles, but also leads to a change in the luminescence of nearby emitters due to interaction with the their near-field. In this regard, optical analysis based on plasmonic nanoparticles can be carried out both through absorption and through fluorescence. The high stability of LSPR allows for long-term tracking of individual plasmonic nanoparticles, which facilitates the detection of transient processes and detailed study of chemical and biological reactions [9].

LSPRs significantly increase the efficiency of photon absorption and scattering. As a result, plasmonic nanoparticles, unlike traditional organic dyes, demonstrate a significantly higher extinction coefficient, which often exceeds that of dyes by several orders of magnitude. LSPRs enhance electric fields near the surface of nanoparticles, with the magnitude of the enhancement depends on the inverse of the distance to the surface. In addition, the LSPR characteristics of nanoparticles can be tuned by varying parameters such as size, morphology, distance between nanoparticles, and properties of the environment [10, 11]. In particular, the aggregation of colloidal plasmonic nanoparticles into clusters can significantly modify the fields on their surface. Recent studies have demonstrated that excited conduction electrons located on the surface of plasmonic nanoparticles are also capable of interacting with the dipoles of nearby luminescent nanoparticles (LNPs) used to detect a specific target molecule, changing their luminescent properties [11, 12]. This interaction can lead to two opposite results: luminescence quenching and enhancement. In particular, the degree of quenching or enhancement caused by LSPR is affected by the LNP characteristics and the distance between the LNP and plasmonic nanoparticles in addition to the LSPR parameters. An increase in the signal level is usually achieved when the LSPR frequency of the metal nanostructure coincides with the LNP excitation frequency. This contributes to an increase in the excitation intensity due to the localization of the electromagnetic field near the metal nanostructure. An increase in the luminescence intensity can also be realized by increasing the rate of radiative transition of emitters, which is known as the Purcell effect [13]. This effect is observed when the LSPR frequency of the metal nanostructure coincides with the radiation frequency of the LNP.

In addition to enhancing luminescence, this condition can lead to non-radiative resonant energy transfer (RET) from the donor ion to the metal nanostructure through their near fields. This interaction can cause luminescence quenching, known as the Förster effect [14, 15]. Most studies indicate that the luminescence of LNPs is enhanced by interaction with various types of plasmonic metal nanostructures, such as silver periodic nanogratings [16], gold pyramids, nanoholes, nanorods and planar triangular nanoantennas [17–20]. A 20-30-fold enhancement of the fluorescence of labeled biomarkers on cells was also demonstrated using plasmonic gold nanoisland films [9]. A significant Purcell factor ($\sim$100) and a limiting detection concentration of 3.1 pmol/L were demonstrated using a system consisting of an organic label and an Au/Ag

oligomer [21]. In the work [22], the influence of the geometry and number of NPs in Au oligomers on the luminescence of organic label was studied, but the authors did not distinguish Purcell effect from other causes of decay rate increasing. However, luminescence quenching has also been observed in other studies. For example, Zhang et al. [23] reported a decrease in the luminescence brightness of 120 nm diameter LNPs with a 20 nm thick silica shell when interacting with 9.4 nm diameter gold nanoparticles. Luminescence quenching due to non-radiative RET in LNPs has also been demonstrated when interacting with gold nanoparticles of similar or smaller size [24, 25].

In the context of the above, plasmon-enhanced luminescence is the result of the influence of many factors. In particular, the sensitivity of LSPR to the surrounding analyte molecules can be used. In our work, nanoclusters are considered, the cores of which are LNPs of $CeYTbF_3$ surrounded by gold nanoparticles (AuNP). The luminescence of these LNPs occurs due to transitions from the $^5D_4$ level to the sublevels of the ^7F state [26]. The wavelengths of the four observed transitions are approximately 490 nm, 540 nm, 590 nm and 620 nm. These lines are partially or completely overlapped by the LSPR band of AuNP, which enables Purcell effect. This system can be synthesized in a colloidal solution and then deposited on a substrate. An idea arises to use such structures as labels for immunoassay of biologically significant analytes both in liquid and in the form of special substrates for analysis. Radachlorin, which has absorption bands in the violet and red-orange regions of the visible spectrum, is considered as a test analyte in the work. Among the extensive set of experimental data on the control of particle luminescence using plasmonic nanostructures, two main aspects are distinguished that determine the unique properties of hybrid systems: the size and shape of the subsystems, as well as the distance between them. Our main goal is to characterize from a fundamental perspective the possibility of plasmonic enhancement of luminescence as the number of plasmonic nanoparticles and their configuration change. This will allow us to predict the average Purcell factor and to determine the configurations that contribute most to the luminescence enhancement for different concentrations of AuNPs and their ratio to the concentration of LNPs. This will be a significant step in the development of nanosensors based on luminescence quenching or enhancement.

1. Simulation parameters and conditions

Simulation of plasmonic enhancement of spontaneous emission (Purcell effect) in a nanocluster was carried out, consisting of a core – a dielectric particle of $CeYTbF_3$ phosphor with a radius of 10 nm and ligands surrounding the core – plasmonic AuNP with a radius of 47 nm, coated with a polyethyleneimine (PEI) shell with a thickness of 4 nm. The polymer shell was used as a linker between the core and ligands, as well as to reduce the influence of near-field energy transfer (Förster effect). Radachlorin was considered as a possible analyte near the examined system. The finite-difference time-domain (FDTD) method was used. The size of the simulation region was 600x600x650 nm, the cell size of the computational grid was 4 nm, and a denser grid with a cell size of 1 nm was set on the objects. The refractive index of the surrounding space was chosen to be constant and equal to 1.33 (water). The boundary conditions chosen were perfectly matched layers (PML) with a total of 8 layers with a standard profile in the stretched-coordinate formulation. To mitigate the consequences of the staircasing approximation of non-flat surfaces on a Cartesian computational grid, a conformal sub-pixel smoothing algorithm was applied. The dielectric permittivity of the phosphor was specified using the Lorentz model:

$$\varepsilon = \varepsilon_d + \frac{Ne^2}{m\varepsilon_0} \frac{f_{osc}}{\omega_0^2 - \omega^2 - i\omega\gamma} \tag{1}$$

where $\varepsilon_d = 2$ is the dielectric permittivity of the crystalline matrix, $N = 10^{21}$ см$^{-3}$ is the concentration of Tb ions, $f_{osc} = 6 \cdot 10^{-8}$ is the oscillator strength of the transition from the ground state to the $^5D_4$ level [27, 28], ω_0 and γ are the cyclic frequency and linewidth, taken from the experimental spectrum [26], m, e are the mass and charge of the electron. The dielectric permittivity of gold was taken from the CRC Handbook [29]. Tabulated values are approximated by built-in models of the simulation software (Ansys Lumerical FDTD). The refractive index of the polymer linker shell (PEI) was assumed constant and equal to 1.52 [30].

The Purcell factor was calculated as the ratio of local densities of electromagnetic states in the presence and absence of plasmonic nanoparticles. The power emitted by a unit point light source was calculated for this. The local density of states is defined by the formula:

$$\rho_\mu(\mathbf{r}, \omega) = \frac{6\omega}{\pi c^2} \left\{ \mathbf{n}_\mu \cdot \mathrm{Im} \left[\hat{G}(\mathbf{r}, \mathbf{r}, \omega) \right] \cdot \mathbf{n}_\mu \right\} \tag{2}$$

where c is the speed of light in vacuum, $\mathbf{n}_\mu$ is the unit vector in the direction of the dipole moment, $\hat{G}$ is the total dyadic Green's function for the electric field. The light source was a point dipole located at the center of the LNP. The range of emitted wavelengths was 300–800 nm. As follows from the Eq. (2), the Purcell effect depends on the Green's function, which means the enhancement of luminescence is influenced by the environment. For the sensor to be most sensitive to the presence of a specific analyte, the absorption bands of the analyte should fall within the band of the LSPR. In this case, the influence of the analyte on the Purcell effect will be greatest, potentially shifting the peak of luminescence enhancement.

2. Modeling of different configurations of Au ligands surrounding a $CeYTbF_3$ nanoparticle on an Au substrate

In order to achieve a significant change in the Purcell effect in the presence of one or more analyte molecules near a nanoparticle or nanocluster, it is necessary to use structures with LSPR in the analyte absorption region. To find structures with such properties, we simulated the plasmonic enhancement of spontaneous emission in a system consisting of one dielectric particle of the $CeTbF_3$ phosphor and a different number (from 1 to 5) of AuNPs coated with a PEI shell and lying on an Au substrate.

The number of all simulated configurations of the ligand arrangement around the LNP was 7: there were 1 configuration with one AuNP, 1 with two AuNPs, 2 with three AuNPs, 2 with four AuNPs, and 1 with five AuNPs.

In the first configuration, one AuNP and a LNP were positioned vertically one above the other relative to the Au substrate, with the AuNP being closer to the substrate surface. The dipole moment of the source was directed along the vertical axis of the nanocluster, perpendicular to the substrate surface (Fig. 1(a)). In this configuration, the plasmon resonance was in the green region of the visible spectrum. In the second configuration, two AuNPs and a LNP lay on the surface of an Au substrate on one straight line, the dipole moment of the source was directed parallel to the substrate surface (Fig. 1(b)). The main peak of the plasmon resonance was also in the green region of the visible spectrum, but, in addition, there were also bands in the red-orange region.

In the configuration with three AuNPs, the ligands were arranged on the substrate surface in such a way that they formed an isosceles triangle, with the LNP located at its center. The dipole moment was oriented parallel to the substrate surface and parallel (blue curve) or perpendicular

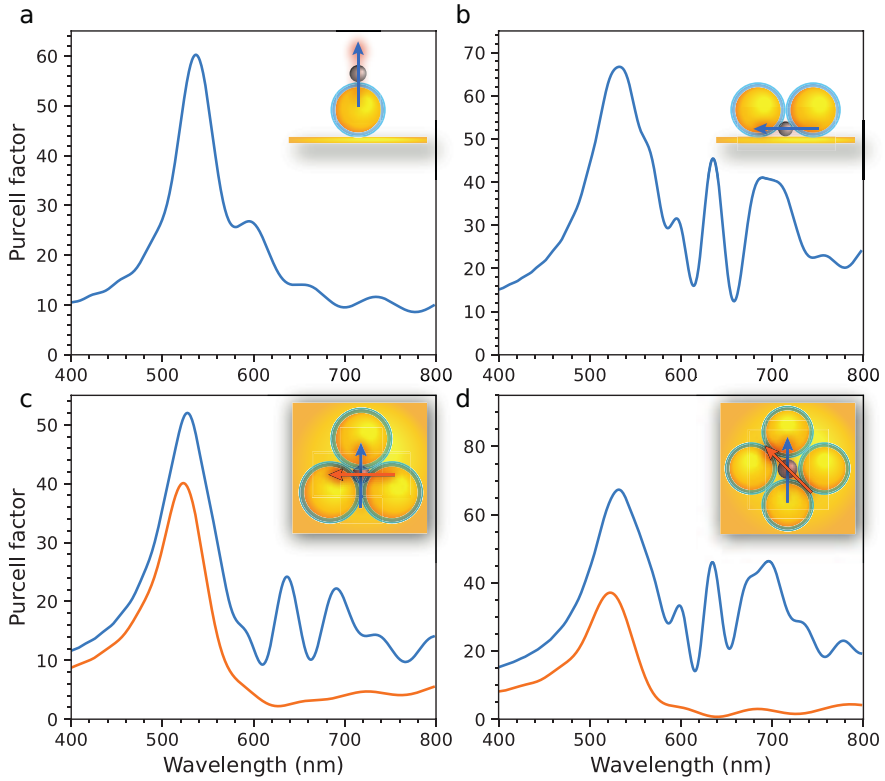

Fig. 1. The Purcell factor: (a) in the presence of one ligand on the Au substrate with the source dipole moment oriented along the vertical axis of the nanocluster, perpendicular to the substrate surface, (b) in a linear configuration of 2 ligands on the Au substrate with the source dipole moment oriented parallel to the line of connection of AuNPs, (c) in a triangular configuration of 3 ligands on the Au substrate with the source dipole moment oriented along the height (blue curve) and perpendicular to the height (orange curve) of the triangle, (d) in a square configuration of 4 ligands on the Au substrate with the source dipole moment oriented along the side (blue curve) and the diagonal (orange curve) of the square. The insets show the nanocluster geometry (side view for (a-b) and top view for (c-d)

(orange curve) to the height of the triangle. The Purcell factor for this configuration are presented in Fig. 1(c).

In the configuration with four AuNPs, the ligands were arranged on the surface of the Au substrate to form a square, with the LNP at its center. The dipole moment was oriented parallel to the substrate surface along the side (blue curve) or the diagonal (orange curve) of the square. Fig. 1(d) shows the Purcell factor in this configuration.

In the configuration with five AuNPs, the ligands were located on the surface of the Au substrate, forming a regular quadrangular pyramid, the LNP was in the center of the pyramid. The dipole moment was oriented parallel to the surface of the substrate along the diagonal of the pyramid base. A schematic representation of this configuration (side view) is shown in Fig. 2. It should be noted that the spectrum contains additional plasmon resonance peaks at other wavelengths, which is due to the fact that the geometry of this cluster supports several

plasmon resonance modes. When using radachlorin as an analyte, configurations with four and five AuNPs on a substrate are optimal, since they exhibit a plasmonic enhancement peak that coincides with the long-wavelength absorption region of radachlorin.

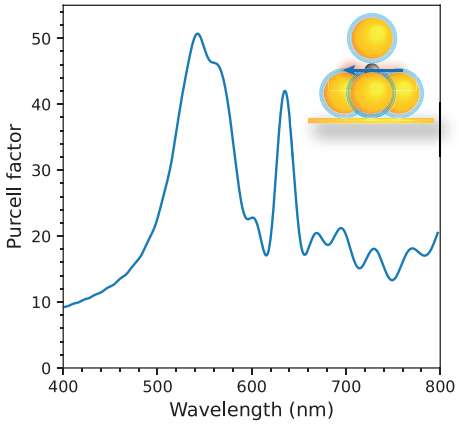

Fig. 2. Purcell factor in a configuration with 5 AuNPs forming a regular quadrangular pyramid with the LNP in the center, on an Au substrate. The dipole moment was oriented parallel to the substrate surface along the diagonal of the pyramid base. The inset shows a schematic representation of the system configuration (side view)

3. Modeling of different configurations of Au ligands surrounding a $CeYTbF_3$ nanoparticle in a colloidal solution

In order to clarify the overall picture of luminescence enhancement in a colloidal solution, the simulations of plasmonic enhancement of spontaneous emission were performed in a system consisting of one dielectric particle of the $CeTbF_3$ phosphor and a different number (from 1 to 4) of Au ligands in nonequivalent configurations. The number of all simulated configurations of the arrangement of AuNPs around the phosphor was 19, of which there were 1 configuration with one nanoparticle, 4 with two AuNPs, 7 with three AuNPs, and 7 with four AuNPs. In the case of two AuNPs, we simulated the local density of states in the following configurations:

2.1. Two AuNPs are adjacent to the LNP along the diameter, the source dipole moment vector is parallel to the system axis;

2.2. Two AuNPs are adjacent to the LNP and touch each other, forming a dimer, the dipole moment is directed towards the center of one of the AuNP of the dimer;

2.3. Two AuNPs are adjacent to the LNP and are in contact with each other, forming a dimer, the dipole moment is directed perpendicular to the direction of the center of one of the AuNPs;

2.4. Two AuNPs are adjacent to the LNP and are in contact with each other, forming a dimer, the dipole moment is parallel to the dimer axis.

In the case of three gold particles, we performed numerical simulation of the local density of states in the following configurations:

3.1. The third AuNP is added to the configuration 2.1 adjacent with one of the AuNPs along the diameter;

3.2. Three AuNP are adjacent each to the LNP and placed at the vertices of the isosceles triangle, which lateral sides are formed by contacting AuNP, the source dipole moment is oriented along the height of the isosceles triangle;

3.3. Similar to the configuration 3.2, but the source dipole moment is oriented parallel the base of the isosceles triangle formed by the centers of AuNPs;

3.4. Similar to the configuration 3.2, but the source dipole moment is oriented parallel the leg of the isosceles triangle formed by the centers of AuNPs;

3.5. Three AuNPs are in contact and are located at the vertices of the square, in the center of which is the LNP, leaving one corner of the square free; the dipole moment is directed along the diagonal of the square;

3.6. The third AuNP is added to the configuration 2.1 adjacent with both of the AuNPs, but no touching LNP, the source dipole moment is oriented along the base of the acute-angled isosceles triangle formed by the centers of AuNPs;

3.7. Three AuNPs are in contact and are located at the vertices of obtuse-angled isosceles triangle, the LNP occupies the base center, contacting only the middle AuNP (at the obtuse angle), the source dipole moment is oriented along the base of the triangle;

In the case of four AuNPs, we modeled the local density of states in the following configurations:

4.1. Two dimers of AuNPs are arranged along the diameter of the LNP, touching it so that the centers of all five nanoparticles lie on the same line; the dipole moment of the source is parallel to the axis of the system;

4.2. The fourth AuNP is added at the free corner of the square in the configuration 3.5, the dipole moment of the source is directed parallel to the side of the square;

4.3. Similar to the configuration 4.2, but the source dipole moment is directed parallel to the diagonal of the square;

4.4. The four contacting AuNPs are located at the corners of a rhombus and the LNP occupies the center, touching two AuNPs and forming the minor diagonal of the rhombus; the dipole moment of the source is directed parallel to the major diagonal of the rhombus;

4.5. Similar to the configuration 4.4, but the dipole moment of the source is directed parallel to the minor diagonal of the rhombus;

4.6. Two dimers are each contacting the LNP by all their AuNPs so that the axes of the dimers are mutually perpendicular, and they themselves form two of the six edges of a tetrahedron with the LNP in the center; the dipole moment of the source is oriented orthogonally to the axes of both dimers;

4.7. Similar to the configuration 4.6, but the source dipole moment is oriented parallel to the axis of one dimer and perpendicular to the axis of the other dimer.

Several plasmon resonance modes were observed in clusters of plasmonic nanoparticles. For each configuration, the positions and values of the Purcell factor function were found in no more than two most intense maxima of the spectrum. The results are shown in Fig. 3(a). In most configurations, the plasmon resonance peak is in the green part of the visible spectrum. Due to the large inhomogeneity of the field near the contacts of AuNPs, plasmon resonance peaks at other wavelengths are also observed in the spectrum. For example, in the configurations 2.4, 4.2 and 4.4, the main plasmon resonance peak is located in the orange part of the spectrum, and in the configuration 4.5, both plasmon resonance peaks (green and orange) have approximately the same intensity. For instance, the Purcell factor for different configurations of two AuNPs are given in Fig. 3(b).

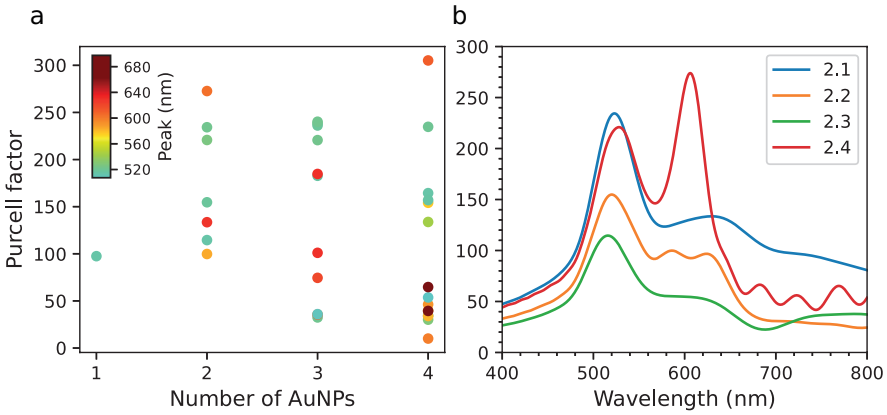

Fig. 3. (a) Purcell enhancement factor as a function of the number of AuNPs for different configurations of their arrangement. The wavelength of the plasmon resonance peaks is shown in color. (b) Purcell enhancement factor for different configurations of two AuNP as a function of wavelength

Conclusion

The study yielded interesting results concerning plasmonic enhancement of spontaneous emission in Au-CeYTbF$_3$ colloidal nanoclusters. Modeling of various AuNP configurations showed that the number and spatial arrangement of nanoparticles relative to each other significantly affect plasmonic resonances and, accordingly, the luminescence efficiency. The Purcell factor at the peak of plasmonic resonance in the most nanocluster configurations reaches about a hundred.

In the studied configurations, the main peaks of plasmon resonance were observed, which were mainly located in the green part of the visible spectrum. This peak is associated with the main dipole mode of plasmon resonance of nanoparticles. However, depending on the geometry of the nanoclusters, peaks were also recorded at other wavelengths, which indicates a complex nature of interactions between nanoparticles. There are configurations where plasmon resonance is observed in the red-orange region of the visible spectrum. This is also a dipole resonance, but not in individual particles, but in the cluster as a whole. In this case, the remaining peaks are associated with the excitation of a higher order multipolar resonances. As a consequence, the optical near-field of these modes decays in space much faster.

Numerical simulation of clusters on the Au substrate showed that there also can be excited several plasmon resonance modes. The substrate acts as a mirror, as if doubling the number of particles, thereby leading to greater inhomogeneity in the space of the exciting field, and this in turn leads to the excitation of modes of greater multipolarity, while the field has a greater localization in the space between the particles. If it is necessary to control the symmetry of individual configurations, the system of clusters on a substrate looks preferable. In addition, a nanocluster located on a substrate leads to the excitation of surface plasmons on its surface, thereby part of the energy leaks away. Therefore, for these systems, a smaller value of the Purcell factor is observed than in colloidal nanoclusters.

The best results in terms of plasmonic enhancement were obtained for configurations with four and five AuNPs, where the plasmonic enhancement peaks coincided with the long-wavelength absorption region of radachlorin.

The study allows us to determine the number of particles in a cluster that is required for a given analyte to produce plasmonic resonance in the desired region. Specific configurations can be controlled in the case of a nanocluster on a substrate, but cannot be controlled in a colloidal solution. Thus, by changing the particle size and changing the concentration of plasmonic particles, it is possible to tune the sensor for a specific desired substance. Given the importance of the spatial distribution and orientation of nanoparticles, further research can focus on optimizing the configurations and studying the effect of the ligand material on the plasmonic resonance of the nanoparticle cluster, which will improve the performance of future sensor systems.

This paper has been supported by the Kazan Federal University Strategic Academic Leadership Program "Priority 2030".

References

[1] K.P.Carter, Fluorescent sensors for measuring metal ions in living systems, *Chem. Rev.*, **114**(2014), 4564–4601. DOI: 10.1021/cr400546e

[2] Y.Han, Inorganic nanoparticles as donors in resonance energy transfer for solid-phase bioassays and biosensors, *Langmuir*, **33**(2017), no. 45, 12839–12858. DOI: 10.1021/acs.langmuir.7b01483

[3] J.Beik, Gold nanoparticles in combinatorial cancer therapy strategies, *Coord. Chem. Rev.*, **387**(2019), 299–324. DOI: 10.1016/j.ccr.2019.02.025

[4] Y.-W.Lin, Gold nanoparticle probes for the detection of mercury, lead and copper ions, *Analyst*, **136**(2011), no. 5, 863–871. DOI: 10.1039/c0an00652a

[5] X.Huang, Gold nanoparticle based platforms for circulating cancer marker detection, *Nanotheranostics*, **1**(2017), no. 1, 80. DOI: 10.7150/ntno.18216

[6] K.Saha, Gold nanoparticles in chemical and biological sensing, *Chem. Rev.*, **112**(2012), no. 5, 2739–2779. DOI: 10.1021/cr2001178

[7] W.Zhou, Gold nanoparticles for in vitro diagnostics, *Chem. Rev.*, **115**(2015), no. 19, 10575–10636. DOI: 10.1021/acs.chemrev.5b00100

[8] M.Tian, Recent advances of plasmonic nanoparticle-based optical analysis in homogeneous solution and at the single-nanoparticle level, *Analyst*, **145**(2020), no. 14, 4737–4752. DOI: 10.1039/D0AN00609B

[9] S.Lee, Plasmonic nanostructure-based bioimaging and detection techniques at the single-cell level, *Trends Analyt. Chem.*, **117**(2019), 58–68. DOI: 10.1016/j.trac.2019.05.006

[10] I.S.Che Sulaiman, A review on colorimetric methods for determination of organophosphate pesticides using gold and silver nanoparticles, *Mikrochim. Acta.*, **187**(2020), 1–22. DOI: 10.1007/s00604-019-3893-8

[11] D.Mendez-Gonzalez, Control of upconversion luminescence by gold nanoparticle size: from quenching to enhancement, *Nanoscale*, **11**(2019), no. 29, 13832-13844. DOI: 10.1039/c9nr02039j

[12] M.Kushlyk, Enhancement of the YAG:Ce,Yb down-conversion emission by plasmon resonance in Ag nanoparticles, *J. Alloys Compd.*, **804**(2019), 202–212. DOI:10.1016/j.jallcom.2019.06.382

[13] E.M.Purcell, Spontaneous emission probabilities at radio frequencies, Springer, (1995), 839.

[14] T.Förster, Zwischenmolekulare energiewanderung und fluoreszenz, *Ann. Phys.*, **437**(1948), no. 1-2, 55–75. DOI: 10.1002/ANDP.19484370105

[15] J.Fan, Energy transfer cassettes based on organic fluorophores: construction and applications in ratiometric sensing, *Chem. Soc. Rev.*, **42**(2013), no. 1, 29–43. DOI: 10.1039/c2cs35273g

[16] D.Lu, Plasmon enhancement mechanism for the upconversion processes in $NaYF_4$:Yb^{3+},Er^{3+} nanoparticles: Maxwell versus Förster, *ACS Nano*, **8**(2014), no. 8, 7780–7792. DOI: 10.1021/nn5011254

[17] Q.C.Sun, Plasmon-enhanced energy transfer for improved upconversion of infrared radiation in doped-lanthanide nanocrystals, *Nano Lett.*, **14**(2014), no. 1, 101–106. DOI: 10.1021/nl403383w

[18] M.Saboktakin, Plasmonic enhancement of nanophosphor upconversion luminescence in Au nanohole arrays, *ACS Nano*, **7**(2013), no. 8, 7186–7192. DOI: 10.1021/nn402598e

[19] N.J.Greybush, Plasmon-enhanced upconversion luminescence in single nanophosphor–nanorod heterodimers formed through template-assisted self-assembly, *ACS Nano*, **8**(2014), no. 9, 9482–9491. DOI: 10.1021/nn503675a

[20] G.Yi, Systematic investigation of the wavelength-dependent upconversion enhancement induced by single plasmonic nanoparticles, *J. Phys. Chem. C*, **122**(2018), no. 24, 13047–13053. DOI:10.1021/acs.jpcc.8b02437

[21] Z.Zhu, Plasmon-enhanced fluorescence in coupled nanostructures and applications in DNA detection, *ACS Appl. Bio Mater.*, **1**(2018), no. 1, 118–124. DOI: 10.1021/acsabm.8b00032

[22] P.Moutet, Surface-enhanced spectroscopy on plasmonic oligomers assembled by AFM nanoxerography, *Nanoscale*, **7**(2015), no. 5, 2009–2022. DOI: 10.1039/c4nr05092d

[23] S.Z.Zhang, Reversible luminescence switching of $NaYF_4$:Yb,Er nanoparticles with controlled assembly of gold nanoparticles, *Chem. Comm.*, **18**(2009), no. 18, 2547–2549. DOI: 10.1039/b823453a

[24] Q.Wu, An upconversion fluorescence resonance energy transfer nanosensor for one step detection of melamine in raw milk, *Talanta*, **136**(2015), 47–53. DOI: 10.1016/j.talanta.2015.01.005

[25] K.Saha, Modification of $NaYF_4$:Yb,Er@SiO_2 nanoparticles with gold nanocrystals for tunable green-to-red upconversion emissions, *J. Phys. Chem. C*, **115**(2011), no. 8, 3291–3296. DOI:10.1021/jp110603r

[26] M.S.Pudovkin, CeF_3-TbF_3-YF_3 nanoparticles for ratiometric temperature sensing, *Opt. Mater.*, **148**(2024), 114831. DOI: 10.1016/j.optmat.2024.114831

[27] E.A.Seregina, Spectral and luminescent characteristics of trivalent lanthanide ions in a $POCl_3$-$SnCl_4$ inorganic solvent, *Opt. Spectrosc.*, **116**(2014), no. 3, 438–453. DOI: 10.1134/S0030400X14020209

[28] I.A.Terra, Judd-Ofelt analysis of Tb^{3+} and upconversion study in Yb^{3+}-Tb^{3+} co-doped calibo glasses, *Chem. Rev.*, **43**(2020), 188–193. DOI: 10.21577/0100-4042.20170465

[29] J.R.Ramble, Handbook of Chemistry and Physics, CRC Press ed,(2021).

[30] L.R.Ip, Loss of INPP4B causes a DNA repair defect through loss of BRCA1, ATM and ATR and can be targeted with PARP inhibitor treatment, *Oncotarget*, **6**(2015), no. 12, 10548. DOI: 10.18632/oncotarget.3307

Эффекты ближнеполевого взаимодействия в коллоидных нанокластерах Au-$CeYTbF_3$ при плазмонном иммуноанализе

Элина А. Избасарова
Алмаз Р. Газизов
Институт физики
Казанский федеральный университет
Казань, Российская Федерация

Аннотация. В данной статье исследуются эффекты плазмонного усиления спонтанного излучения в коллоидных нанокластерах, состоящих из золотых наночастиц и люминофора $CeYTbF_3$. С помощью моделирования различных конфигураций наночастиц, покрытых полиэтиленимином, была проанализирована зависимость положения плазмонных резонансов от их количества и расположения. Результаты показали, что оптимальные конфигурации наночастиц значительно усиливают люминесценцию в требуемой области видимого света, что открывает новые возможности для разработки высокочувствительных наносенсоров. В то же время нанокластеры, расположенные на золотой подложке, демонстрируют меньший коэффицент усиления люминесценции, обладая при этом более неоднородным распределением ближнего оптического поля. Полученные результаты раскрывают зависимость коэффициента усиления люминесценции от пространственного распределения и координационного числа плазмонных наночастиц в нанокластере. Данное исследование вносит вклад в понимание механизмов плазмонного взаимодействия и его применения в области оптического иммуноанализа и биомедицинских технологий.

Ключевые слова: плазмонные наночастицы, эффект Парселла, эффект Ферстера, моделирование методом FDTD, люминесцентные наночастицы.